ACS APPLIED MATERIALS & INTERFACES

www.acsami.org

Research Article

Deep Well Trapping of Hot Carriers in a Hexagonal Boron Nitride Coating of Polymer Dielectrics

Thomas Linker,[#] Yifei Wang,[#] Ankit Mishra, Deepak Kamal, Yang Cao,* Rajiv K. Kalia, Aiichiro Nakano,* Rampi Ramprasad, Fuyuki Shimojo, Gregory Sotzing, and Priya Vashishta

Cite This: *ACS Appl. Mater. Interfaces* 2021, 13, 60393−60400

Read Online

ACCESS | Metrics & More | Article Recommendations | Supporting Information

ABSTRACT: Polymer dielectrics can be cost-effective alternatives to conventional inorganic dielectric materials, but their practical application is critically hindered by their breakdown under high electric fields driven by excited hot charge carriers. Using a joint experiment−simulation approach, we show that a 2D nanocoating of hexagonal boron nitride (hBN) mitigates the damage done by hot carriers, thereby increasing the breakdown strength. Surface potential decay and dielectric breakdown measurements of hBN-coated Kapton show the carrier-trapping effect in the hBN nanocoating, which leads to an increased breakdown strength. Nonadiabatic quantum molecular dynamics simulations demonstrate that hBN layers at the polymer−electrode interfaces can trap hot carriers, elucidating the observed increase in the breakdown field. The trapping of hot carriers is due to a deep potential well formed in the hBN layers at the polymer−electrode interface. Searching for materials with similar deep well potential profiles could lead to a computationally efficient way to design good polymer coatings that can mitigate breakdown.

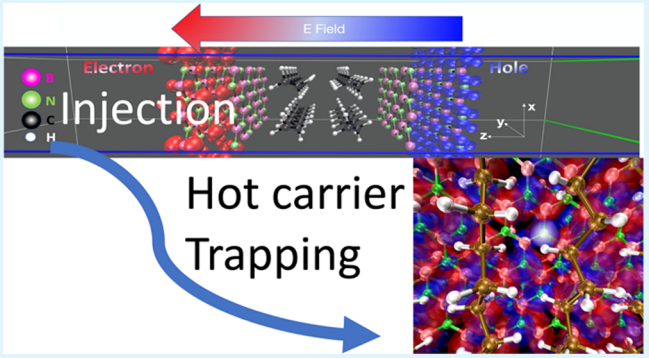

KEYWORDS: *polymer, hexagonal boron nitride, coating, dielectric breakdown, hot carrier, deep well trapping, nonadiabatic quantum molecular dynamics*

INTRODUCTION

Dielectric polymers offer numerous advantages over their inorganic counterparts but are severely limited by their breakdown under high electric fields.[1−8] Dielectric breakdown is typically modeled within the electron avalanche theory,[9−14] where strong electric fields excite hot carriers past the impact ionization energy causing further carriers to be excited (carrier multiplication), which eventually results in structural damage to the polymer and dielectric breakdown.[4,5] To limit the effect of injected hot carriers, there has been a growing effort to utilize nanoscale two-dimensional (2D) materials with large band gaps and favorable electrically insulating capability as coating materials. In the past decade, 2D materials with high breakdown fields, such as hexagonal boron nitride (hBN) (E_b~1200 MV/m),[15] have been widely used to perform nanocoating on polymer dielectrics for significantly enhanced breakdown strength.[16−18] The current hypothesis is that insulating 2D coatings prevent injection of hot charge carriers from the electrode, thus suppressing the leakage current. However, there is a critical lack of mechanistic understanding about the behavior of the charge carriers at the electrode−polymer coating interface as well as a predictive framework to determine good potential nanocoating materials.

Recent theoretical studies using nonadiabatic quantum molecular dynamics (NAQMD) simulations have shed light on the hot carrier dynamics leading to breakdown in dielectric polymers.[19,20] In particular, it was shown that hot carriers can localize at polymer surfaces, thereby causing defect formation and carrier multiplication in a prototypical dielectric polymer, polyethylene (PE).[19] In addition, near the breakdown field, the NAQMD study showed that hot carriers can strongly couple to the C-H vibrational modes in PE, resulting in rapid localization of hot carriers at the surface.[20] This polaronic localization transition is analogous to the coupling of vibrational resonance with Stark shifts of electronic energy levels under an electric field.[20] These studies indicate the necessity to mitigate the strong carrier−phonon coupling and localization of hot carriers in dielectric polymers in order to develop polymers with high breakdown fields.

Received: August 17, 2021
Accepted: December 1, 2021
Published: December 10, 2021

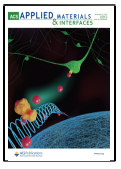

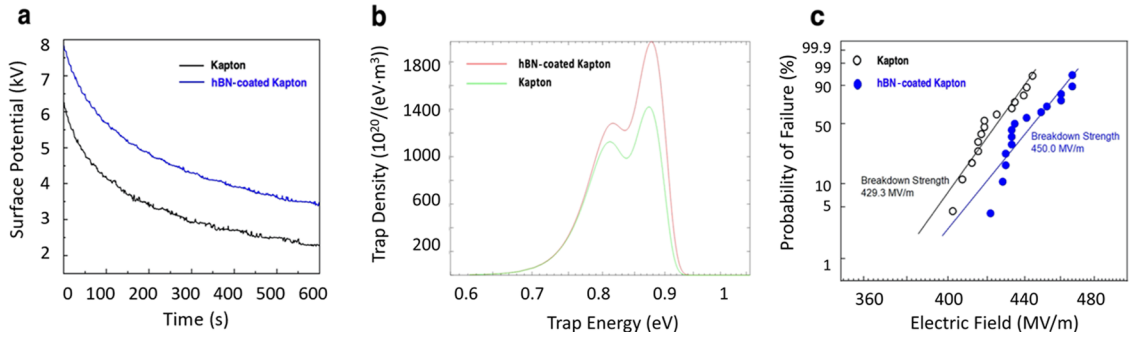

Figure 1. (a) Surface potential decay, (b) trap energy, and (c) Weibull breakdown strength of Kapton and hBN-coated Kapton.

Here, we investigate the hot carrier dynamics at the hBN−polymer interfaces with hBN as a nanocoat along the charge injection interface. Surface potential decay and dielectric breakdown measurements of the commercial polymer Kapton coated with hBN indicate a carrier-trapping effect that leads to an enhanced breakdown field. To investigate the microscopic mechanisms behind this enhancement, a NAQMD simulation was performed at the hBN−polymer electrode interface. The simulation reveals the formation of a deep potential well in the hBN coat, which can trap hot carriers, potentially mitigating their damage. The application of the hBN coat also results in a substantial decrease in the carrier relaxation rate in comparison to previous studies, which is indicative of a weak carrier−phonon interaction. This weak carrier−phonon interaction suggests the potential of hBN to mitigate the detrimental polaronic effects seen to enhance the hot carrier damage.[20] In addition, the signature deep well formed by the hBN layers can readily be calculated with a standard density functional theory (DFT) formalism. This key feature can thus be used as a qualitative proxy for designing a rational search of effective coating materials.[3,8,20,21]

RESULTS

We experimentally observed the carrier-trapping effect in an hBN-coated Kapton film by a surface potential decay measurement, where the polymer film was charged under a high voltage of 6 kV, and the surface potential was monitored by a Kelvin probe. Compared with uncoated Kapton, coated Kapton delivers a higher initial value of surface potential, indicating that more carriers are trapped due to the existence of the hBN nanocoating, as shown in Figure 1a. While the surface potential decays with time in both samples, it could be found that the surface potential of the coated Kapton is always higher than that of the uncoated one, implying that such a carrier-trapping effect could play a significant role in controlling the charge carrier dynamics. To further assess the effects of hBN to trap hot carriers, we calculated the trap energy based on the theory of isothermal surface potential decay.[23] As seen in Figure 1b, a larger trap density can be found after coating BN for both shallow and deep traps. This further demonstrates the charge trapping effect of BN. As the surface potential decay rates can be highly sensitive to the test setup,[24] a detailed explanation of the test setup is provided in the Methods section. Nevertheless, the relative decay rates of uncoated and coated Kapton are expected to be similar regardless of the test setup.

The dielectric insulation of polymers is fundamentally dictated by charge carrier injection and transport. It is believed that the electrical conduction could be suppressed when charge carriers are trapped in deep wells, thus contributing to enhanced insulation properties. To investigate this, we performed dielectric breakdown measurements for coated and uncoated Kapton films. Figure 1c shows that the breakdown strength of coated Kapton is higher than that of the uncoated polymer, which is due to the carrier-trapping effect induced by the hBN nanocoating. To ensure that the enhanced breakdown was attributed to hBN, a scanning electron microscopy (SEM) image of the hBN-coated Kapton is provided in the Supporting Information, Figure S1. We could see the uniform distribution of BN coatings on Kapton at a very large scale, and no obvious aggregation can be seen. Similar to the surface potential decay, the exact value of the breakdown strength is highly associated with the setup of the experiment such as the ramping rate.[25] A detailed description of the experimental setup is provided in the Methods section.

To gain a mechanistic understanding of how hBN nanocoats could enhance polymer breakdown, we performed static DFT and NAQMD simulations to characterize the hot carrier dynamics in the electrode−hBN−polymer interface in a quantum mechanical fashion. Polyethylene (PE) and aluminum (Al) were chosen as standard polymer and electrode materials to assess the effectiveness of the hBN coating as their interface is best characterized both experimentally and computationally.[3,19−21,26−30] As standard electrode/polymer databases use PE/Al as the baseline, with which other polymers and electrodes are assessed,[20−22,28−30] they can thus provide a practical computational screening platform for determining coating materials in the future. While the band alignment varies for different hBN-coated polymers, charge trapping by hBN is expected to remain operative. Thus, PE provides a computationally efficient benchmark for characterizing effective coating materials.

To understand the potential charge injection, we first determined the local potential profiles and band alignment of aluminum, hBN, and PE using DFT.[31−33] To determine the potential profiles and band energies, each material was optimized separately with 30 Å of vacuum applied along the *z*-axis (*c* crystallographic axis) with the Perdew−Burke−Ernzerhof (PBE)[34]-styled generalized gradient approximation (GGA) within the projected augmented wave (PAW) method.[35] Full details of the electronic structure calculation are described in the Methods section. The local potential energy, valence band maximum (VBM), conduction band minimum (CBM), and Fermi level energies were then computed with respect to the mean vacuum energies for each system. Periodic boundary conditions were applied along all three crystallographic directions. The optimized systems are illustrated in Figure 2a. For aluminum, structural optimization

https://doi.org/10.1021/acsami.1c14587
ACS Appl. Mater. Interfaces 2021, 13, 60393−60400

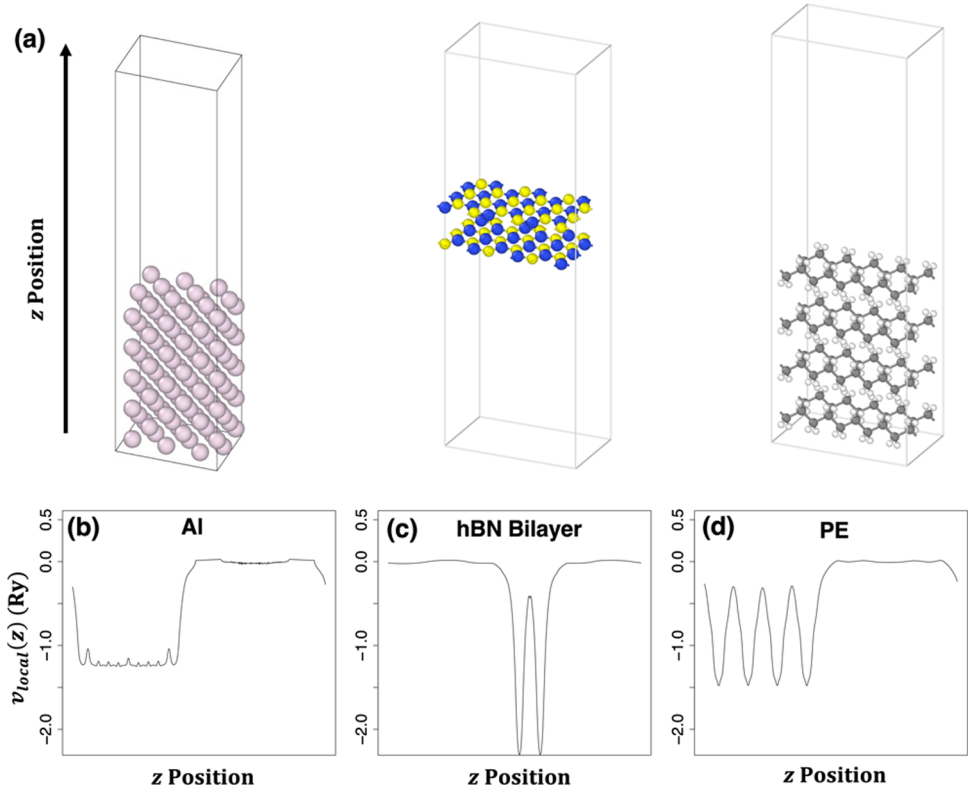

Figure 2. Optimized structures and local potential profiles. (a) Optimized Al, hBN, and PE structures used to compute the local potential and band alignment. Al, B, N, C, and H atoms are colored in silver, blue, yellow, gray, and white, respectively. (b–d) Laterally (*xy*) averaged local potential profiles along the surface normal (*z*) direction.

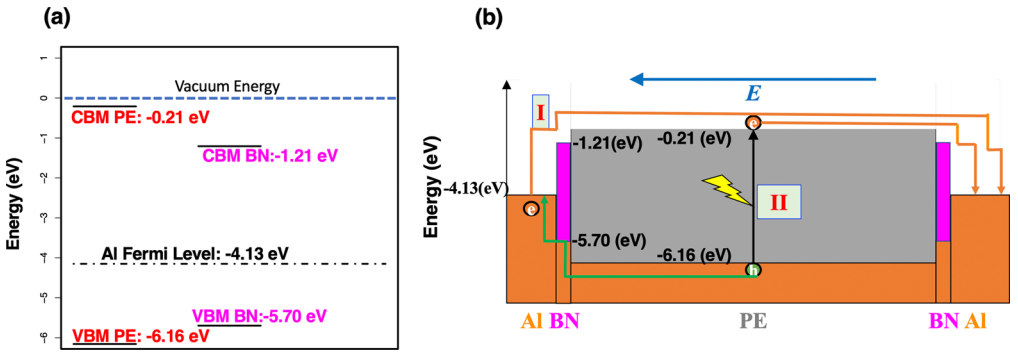

Figure 3. Band alignment and schematic of the charge injection experiment. (a) Computed band alignment with the PBE functional for Al, hBN, and PE with VBM, CBM, and Fermi energy levels labeled. (b) Schematic of the breakdown experiment, where hot carriers can either be (I) directly injected into the polymer at the electrode interface or (II) caused by excitation of secondary electron–hole pairs in the bulk of the polymer.

was performed for a supercell consisting of 2× 3 ×5 symmetrized 4-atom cubic unit cells (instead of a 1-atom trigonal unit cell). For PE, a 2 ×5 ×4 supercell was optimized, where the polymer chain direction is along the *y*-axis (*b* crystallographic axis), resulting in eight total PE chains. For hBN, a 72-atom bilayer system (18 unit cells per layer) was optimized. Figure 2b–d shows the laterally (i.e., *xy*-plane) averaged local potential profiles along the surface normal (*z*) direction for the optimized structures with the mean vacuum energy normalized to zero. A clear Stark deep potential well is formed in the hBN bilayer in comparison to aluminum and PE, indicating the potential for hot carriers to be trapped in hBN layers at the Al–hBN–PE interface.

Figure 3a shows the computed band alignment for the three structures. PE–hBN forms a straddling style band alignment, and the aluminum Fermi level is between the hBN VBM–CBM gap. This indicates that high electric fields lead to the injection of charges from aluminum to hBN at the Al–hBN–PE interface. While the band gap is underestimated using the PBE functional for both hBN and PE, both their relative values are in agreement with the experiment values.[36,37] Figure 3b illustrates the typical breakdown experiment that we model with the NAQMD simulation. Field-induced hot carriers can either be (I) injected directly from the electrode interface into the polymer or (II) introduced through secondary excitations in the bulk of the polymer. Here, we study the hot carrier dynamics described by process I at the hBN–PE interface, whereas process II has extensively been studied using NAQMD simulations.[19,20]

https://doi.org/10.1021/acsami.1c14587
ACS Appl. Mater. Interfaces 2021, 13, 60393–60400

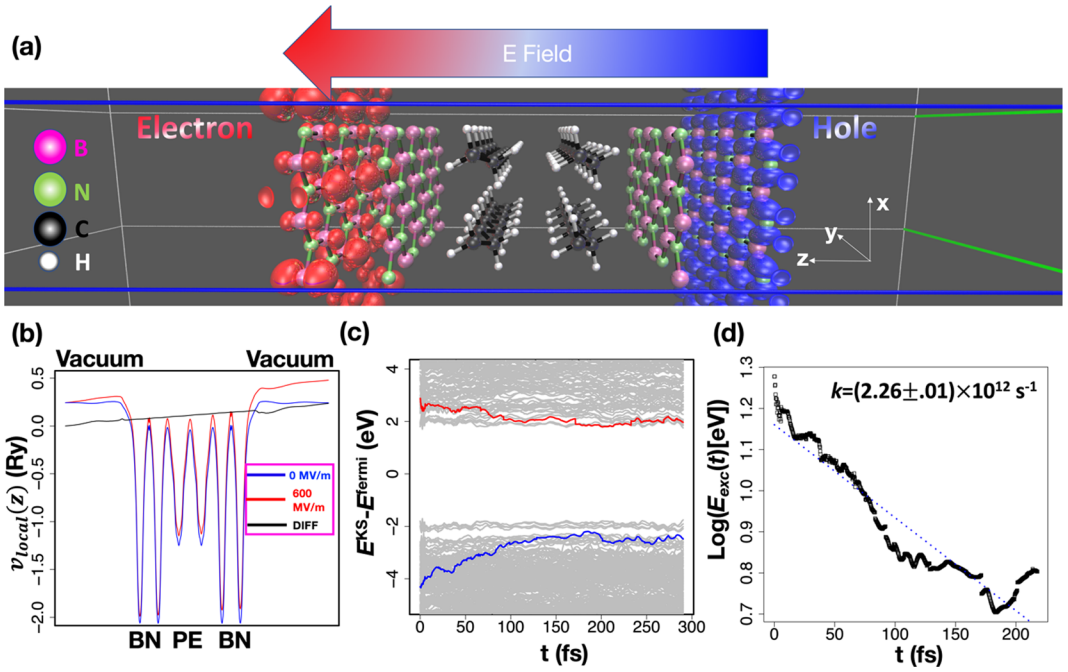

Figure 4. NAQMD simulation. (a) hBN−PE interface used in the NAQMD simulation. B, N, C, and H atoms are colored mauve, lime, black, and white, respectively. Initial excited electron and hole Kohn−Sham (KS) wave functions are colored red and blue, respectively. Electric field was applied along the interface normal direction (z) using a sawtooth potential. (b) Laterally (xy-plane) averaged local potential with (red curve) and without (blue curve) the applied electric field. The difference displaying the linear voltage drop is colored in black. (c) Time evolution of the KS eigenvalues with the hole and electron energies colored in red and blue, respectively. (d) Semi-log plot of the excitation energy vs time (open circles) to estimate the relaxation rate by a linear fit (dotted line).

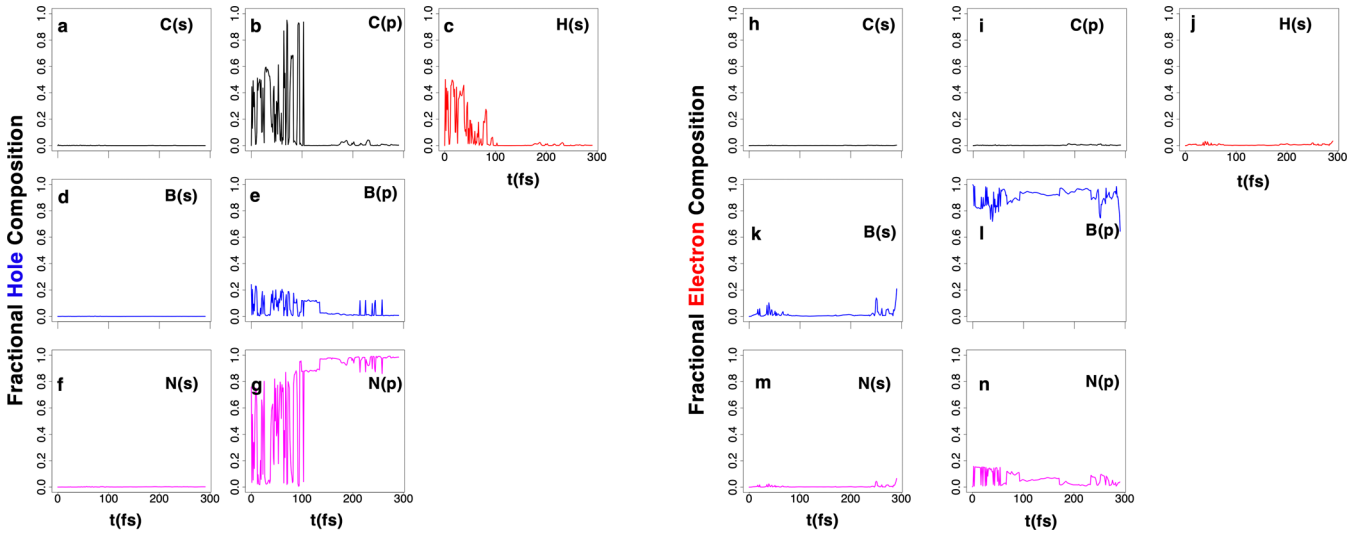

Figure 5. Carrier participation dynamics. (a−g) Angular momentum (l)-dependent fractional contribution of each atomic orbital type to the hole wave function. The hole wave function hops between the C(p) and H(s) PE states and B(p) and N(p) hBN states before localizing to hBN. (h−n) l-dependent fractional contribution of each atomic orbital type to the excited electron wave function, which remains primarily localized in hBN for the entire simulation.

To study the injection of hot carriers from Al at the hBN−PE interface, we performed NAQMD simulation (see Methods section) on the interfacial structure along the (110) plane with 2×5 ×2 unit cells of PE sandwiched between two separate 72-atom bilayers of hBN, which is shown in Figure 4a. A vacuum layer of thickness 15 Å was added to each end of the interface for a total separation of 30 Å to remove spurious interactions between periodic images of the slab. Aluminum was not included in the interface as it merely supplies the initial condition of injection of electrons and holes into the hBN layers, which is modeled in NAQMD as the generation of a high-energy electron−hole pair at the edges of the hBN−PE slab as illustrated in Figure 4a.

To simulate the field-induced hot carrier dynamics, a sawtooth potential was applied along the vacuum direction to simulate the presence of the electric field. An electric field strength of 600 MV/m was used, which is near the breakdown field strength for PE.[5,38] Figure 4b shows the local potential

https://doi.org/10.1021/acsami.1c14587
ACS Appl. Mater. Interfaces 2021, 13, 60393−60400

profiles of the slab with and without the applied electric field and the difference between them. There is a clear linear shift in the local potential as a result of the applied sawtooth potential and the Stark deep potential wells of the hBN layers remain. A similar linear tilt is seen in the spatially projected partial density of states, which is plotted in the Supporting Information, Figure S2. After examining the effect of the field on the local potential, a NAQMD simulation under the electric field was run within the canonical ensemble at a temperature of 300 K with a time step of 0.2418 fs.

Figure 4c shows the time evolution of the KS eigenvalues along the nonadiabatic trajectory with the hole and electron energies colored in blue and red, respectively. The excited hole and electron both slowly relax toward the VBM−CBM energy levels, respectively (∼200 fs). To better quantify the energy loss rate k, we calculated the average electronic excitation energy as a function of time

$$E\mathrm{exc}\,(t) = \frac{\sum_i f_i(t)\epsilon_i(t)\theta(\epsilon_i(t)) - \sum_i (1 - f_i(t))\epsilon_i(t)\theta(-\epsilon_i(t))}{\sum_i f_i(t)\epsilon_i(t)\theta(\epsilon_i(t)) + \sum_i (1 - f_i(t))\epsilon_i(t)\theta(-\epsilon_i(t))} \quad (1)$$

where $f_i(t)$ is the occupation of the ith band at time t, $\epsilon_i(t)$ is the KS energy, and θ is the heavy-side function. The rate k was determined by a semi-log fit of the excitation energy as a function of time over the exponential decay period of the energy (∼200 fs), which is plotted in Figure 3d. The rate k $=(2.26 \pm .01) \times 10^{12}$ s^{-1} is orders of magnitude slower than that reported in a previous NAQMD study of sole PE,[19] which is indicative of a weak carrier−phonon interaction. This indicates that introduction of the hBN layer could limit strong polaronic coupling seen to result in rapid damage to C−C bonds in previous study.[20] As the current study incorporated a much thinner PE layer than that used in previous studies, tunneling effects could play a role in the calculated rate. However, as tunneling is anticipated to cause faster carrier relaxation and surface localization in this study of the hBN−PE interface, the calculated slower rate indicates that the carrier-trapping effect of hBN is far stronger than the potential tunneling effects.

We next examined the carrier dynamics by looking at the l-dependent atomic orbital contributions to electron and hole wave functions as a function of time via Mulliken analysis[39] (Figure 5). Figure 5a−g illustrates that the hole wave function alternates between C(p) and H(s) orbitals and B(p) and N(p) during the first 100 fs. This indicates that the hole wave function hops between the hBN and PE layers for the first 100 fs. After the first 100 fs, the hole wave function is largely composed of N(p) orbitals with a small B(p) orbital composition, indicating that the hole localized and became trapped in the hBN layers for the remainder of the simulation. The fractional excited electron composition is similarly plotted in Figure 5h−n. The excited electron is almost solely composed of hBN states (primarily B(p) orbitals) throughout the entire simulation. This indicates that the electron remains trapped in the hBN deep potential wells for the entire NAQMD trajectory and is unable to damage the polymer. A video of the electron−hole dynamics along the trajectory is provided in the Supporting Information Video S1, which illustrates the localization of the electron and the hole within the hBN layers. Throughout the trajectory, no bond breaking inside the polymer was observed.

CONCLUSIONS

Surface potential measurement implies that the hBN nanocoating could contribute to charge carrier trapping and consequently improve the dielectric insulation of polymers, which is evidenced by the enhanced breakdown strength in hBN-coated Kapton. NAQMD simulations corroborate the ability of hBN layers to trap hot carriers at the hBN−polymer interface. The trapping of hot carriers is a result of deep potential wells formed in the hBN layers. Since local potential profiles relative to the vacuum energy can be efficiently computed with standard DFT calculations, probing this feature in other potential coating materials could provide an efficient rational design principle for general screening of effective polymer coating materials.

For assessing the effectiveness of the coating for specific polymers, it is also desirable to compute the well potential profile of the interface and compare the relative depths especially since charge transfer and polarization effects can happen at the interface with polymers containing nitrogen and oxygen groups. In addition, as previously mentioned, more complex polymers are expected to have different band structures, which could potentially change the charge carrier dynamics. In the preliminary theoretical and experimental study of hBN-coated polycarbonate, however, we have found a similar charge trapping effect of hBN despite the differing band structures compared to the polymers discussed here. The study of polycarbonate goes beyond the scope of this work and will be published elsewhere. While the key point of this study is the deep potential located in the BN coating layer, other experiments such as photocurrent injection measurement can also provide complementary information such as barrier height between the electrode and the polymer as well as the surface states. A recent study of hBN using photocurrent injection measurements has indeed showed the ability of hBN nanocoats to reduce surface states at polymer−metal interfaces,[40] further corroborating the carrier trapping reported here.

METHODS

Experimental Section. To prepare the coating precursor, hexagonal BN nanosheets (US Research Nanomaterials) with a diameter of 800 nm were first dispersed in ethanol by tip sonication for 30 min. Polyvinyl butyral was then dissolved in the above solution by stirring overnight, which acts as the polymer binder in the nanocoating. The solution was tip-sonicated again just before the coating process. A Kapton film with a thickness of 8 μm was purchased from DuPont for the experimental study. The film was cleaned using ethanol and dried at 80 °C. Then, it was dipped into the coating precursor and kept for 30 s before being lift up. The dip-coated film was dried at 80 °C overnight before conducting electrical measurements. Dielectric breakdown tests were carried out using a resistor−capacitor circuit with a linear voltage ramp of 215 V/s. Ball-plate electrodes were adopted to apply high voltage and electrically ground the sample. More than 10 samples of coated and uncoated films were tested to obtain the statistic breakdown strength in the Weibull plot. In the surface potential measurement, a pair of needle-to-plate electrodes was used to conduct corona charge. The distance between the two electrodes is 6 mm. The film sample was placed on the plate electrode that is grounded. A DC voltage of 6 kV was applied on the needle electrode for 1 min. Then the sample was transferred under a Kelvin probe to observe the surface potential decay for 10 min.

DFT Calculation of Band Alignment. Structure optimization for a band alignment calculation was performed till the forces were within 5×10^{-4} Hartree/Bohr. Energies and forces were computed using a plane-wave basis within the PAW method.[35] Projector functions were

https://doi.org/10.1021/acsami.1c14587
ACS Appl. Mater. Interfaces 2021, 13, 60393−60400

generated for the 1s hydrogen, 2s and 2p carbon, 2s and 2p boron, 2s and 2p nitrogen, and 3s, 3p, and 3d Al states. For all structures, a plane-wave cutoff of 35 Ry for the wavefunctions and 300 Ry for the density was used. The gamma point was used to sample the Brillouin zone. The PBE[34]-styled GGA for the exchange−correlation functional was used, and van der Waals interactions were included with the DFT-D method.[41] More accurate calculations of the band gaps and VBM−CBM energies with respect to the vacuum energy can be obtained with the use of hybrid functionals such as the Heyd−Scuseria−Ernzerhof (HSE06) hybrid functional, incorporation of Hubbard interactions in the local density component of the exchange−correlation potential (LDA + U), or even many-body perturbative Green's function methods such as G_0W_0 or GWΓ[1].[37,42−45] However, we were mostly interested in obtaining a qualitative understanding of the charge injection at the metal−hBN−polymer interface to perform NAQMD simulation of the hot carrier dynamics, where these advanced methods become impractical to use. Calculations were performed in the highly parallelized plane-wave-based software QXMD.[46]

NAQMD Simulation. NAQMD simulation was performed at the hBN−PE interface along the (110) plane with 2×5 ×2 unit cells of PE sandwiched between two separate 72-atom bilayers of hBN. Prior to the NAQMD simulation, hybrid cell atomic optimization was performed on the slab until the forces were within 5×10^{-4} Hartree/Bohr and successive energy minimization was within 1×10^{-7} Hartree/atom. NAQMD simulation[47−49] was performed with excited-state forces on atoms computed in the framework of time-dependent DFT[50] with phonon-assisted excited transitions between electronic states modeled within the surface hopping approach.[51,52] The NAQMD algorithm used for the excited-state dynamics is described in refs 46, 47, 49 and was carried out using QXMD software.[46]

■ ASSOCIATED CONTENT

Supporting Information

The Supporting Information is available free of charge at https://pubs.acs.org/doi/10.1021/acsami.1c14587.

Video of electron−hole dynamics at the BN−PE interface (MP4)

SEM image of hBN-coated Kapton and spatially projected partial density of states (PDF)

■ AUTHOR INFORMATION

Corresponding Authors

Yang Cao − *Electrical Insulation Research Center, Institute of Materials Science, University of Connecticut, Storrs, Connecticut 06269, United States;* orcid.org/0000-0001-7034-2792; Email: yang.cao@uconn.edu

Aiichiro Nakano − *Collaboratory for Advanced Computing and Simulations, University of Southern California, Los Angeles, California 90089-0242, United States;* orcid.org/0000-0003-3228-3896; Email: anakano@usc.edu

Authors

Thomas Linker − *Collaboratory for Advanced Computing and Simulations, University of Southern California, Los Angeles, California 90089-0242, United States*

Yifei Wang − *Electrical Insulation Research Center, Institute of Materials Science, University of Connecticut, Storrs, Connecticut 06269, United States;* orcid.org/0000-0002-0848-9977

Ankit Mishra − *Collaboratory for Advanced Computing and Simulations, University of Southern California, Los Angeles, California 90089-0242, United States*

Deepak Kamal − *School of Materials Science and Engineering, Georgia Institute of Technology, Atlanta, Georgia 30332, United States;* orcid.org/0000-0003-1943-7774

Rajiv K. Kalia − *Collaboratory for Advanced Computing and Simulations, University of Southern California, Los Angeles, California 90089-0242, United States*

Rampi Ramprasad − *School of Materials Science and Engineering, Georgia Institute of Technology, Atlanta, Georgia 30332, United States;* orcid.org/0000-0003-4630-1565

Fuyuki Shimojo − *Department of Physics, Kumamoto University, Kumamoto 860-8555, Japan*

Gregory Sotzing − *Institute of Materials Science, University of Connecticut, Storrs, Connecticut 06269, United States*

Priya Vashishta − *Collaboratory for Advanced Computing and Simulations, University of Southern California, Los Angeles, California 90089-0242, United States;* orcid.org/0000-0003-4683-429X

Complete contact information is available at: https://pubs.acs.org/10.1021/acsami.1c14587

Author Contributions

#T.L. and Y.W. contributed equally to this work.

Notes

The authors declare no competing financial interest.

■ ACKNOWLEDGMENTS

This work was supported by the Office of Naval Research through a Multi-University Research Initiative (MURI) grant (N00014-17-1-2656). The simulations were performed at the Argonne Leadership Computing Facility under the DOE INCITE and Aurora Early Science programs and at the Center for High Performance Computing of the University of Southern California.

■ REFERENCES

(1) Chu, B.; Zhou, X.; Ren, K.; Neese, B.; Lin, M.; Wang, Q.; Bauer, F.; Zhang, Q. M. A Dielectric Polymer with High Electric Energy Density and Fast Discharge Speed. *Science* **2006**, *313*, 334.

(2) Ji, D.; Li, T.; Zou, Y.; Chu, M.; Zhou, K.; Liu, J.; Tian, G.; Zhang, Z.; Zhang, X.; Li, L.; Wu, D.; Dong, H.; Miao, Q.; Fuchs, H.; Hu, W. Copolymer Dielectrics with Balanced Chain-Packing Density and Surface Polarity for High-Performance Flexible Organic Electronics. *Nat. Commun.* **2018**, *9*, 2339.

(3) Sharma, V.; Wang, C.; Lorenzini, R. G.; Ma, R.; Zhu, Q.; Sinkovits, D. W.; Pilania, G.; Oganov, A. R.; Kumar, S.; Sotzing, G. A.; Boggs, S. A.; Ramprasad, R. Rational Design of All Organic Polymer Dielectrics. *Nat. Commun.* **2014**, *5*, 4845.

(4) Jones, J. P.; Llewellyn, J. P.; Lewis, T. J. The Contribution of Field-Induced Morphological Change to the Electrical Aging and Breakdown of Polyethylene. *IEEE Trans. Dielectr. Electr. Insul.* **2005**, *12*, 951.

(5) Ieda, M. Dielectric Breakdown Process of Polymers. *IEEE Trans. Electr. Insul.* **1980**, *EI-15*, 206.

(6) Su, H.; Strachan, A.; Goddard, W. A. Density Functional Theory and Molecular Dynamics Studies of the Energetics and Kinetics of Electroactive Polymers: Pvdf and P(Vdf-Trfe). *Phys. Rev. B* **2004**, *70*, 64101.

(7) Li, Q.; Chen, L.; Gadinski, M. R.; Zhang, S.; Zhang, G.; Li, H. U.; Iagodkine, E.; Haque, A.; Chen, L.-Q.; Jackson, T. N.; Wang, Q. Flexible High-Temperature Dielectric Materials from Polymer Nanocomposites. *Nature* **2015**, *523*, 576−579.

(8) Shen, Z.-H.; Wang, J.-J.; Jiang, J.-Y.; Huang, S. X.; Lin, Y.-H.; Nan, C.-W.; Chen, L.-Q.; Shen, Y. Phase-Field Modeling and

Machine Learning of Electric-Thermal-Mechanical Breakdown of Polymer-Based Dielectrics. *Nat. Commun.* **2019**, *10*, 1843.
(9) Zener, C. A Theory of the Electrical Breakdown of Solid Dielectrics. *Proc. R. Soc. A* **1934**, *145*, 523.
(10) Frohlich, A. Theory of Electrical Breakdown in Ionic Crystals. *Proc. R. Soc. A* **1937**, *160*, 230.
(11) Von Hippel, A. Electric Breakdown of Solid and Liquid Insulators. *J. Appl. Phys.* **1937**, *8*, 815.
(12) Sparks, M.; Mills, D. L.; Warren, R.; Holstein, T.; Maradudin, A. A.; Sham, L. J.; Loh, E.; King, D. F. Theory of Electron-Avalanche Breakdown in Solids. *Phys. Rev. B* **1981**, *24*, 3519.
(13) Sun, Y.; Boggs, S. A.; Ramprasad, R. The Intrinsic Electrical Breakdown Strength of Insulators from First Principles. *Appl. Phys. Lett.* **2012**, *101*, 132906.
(14) Sun, Y.; Bealing, C.; Boggs, S.; Ramprasad, R. 50+ Years of Intrinsic Breakdown. *IEEE Electr. Insul. Mag.* **2013**, *29*, 8.
(15) Hattori, Y.; Taniguchi, T.; Watanabe, K.; Nagashio, K. Layer-by-Layer Dielectric Breakdown of Hexagonal Boron Nitride. *ACS Nano* **2015**, *9*, 916−921.
(16) Azizi, A.; Gadinski, M. R.; Li, Q.; AlSaud, M. A.; Wang, J.; Wang, Y.; Wang, B.; Liu, F.; Chen, L.-Q.; Alem, N.; Wang, Q. High-Performance Polymers Sandwiched with Chemical Vapor Deposited Hexagonal Boron Nitrides as Scalable High-Temperature Dielectric Materials. *Adv. Mater.* **2017**, *29*, No. 1701864.
(17) Cui, Z.; Cao, Z.; Ma, R.; Dobrynin, A. V.; Adamson, D. H. Boron Nitride Surface Activity as Route to Composite Dielectric Films. *ACS Appl. Mater. Interfaces* **2015**, *7*, 16913−16916.
(18) Cheng, S.; Zhou, Y.; Hu, J.; He, J.; Li, Q. Polyimide Films Coated by Magnetron Sputtered Boron Nitride for High-Temperature Capacitor Dielectrics. *IEEE Trans. Dielectr. Electr. Insul.* **2020**, *27*, 498−503.
(19) Kumazoe, H.; Fukushima, S.; Tiwari, S.; Kim, C.; Huan, T. D.; Kalia, R. K.; Nakano, A.; Ramprasad, R.; Shimojo, F.; Vashishta, P. Hot-Carrier Dynamics and Chemistry in Dielectric Polymers. *J. Phys. Chem. Lett.* **2019**, *10*, 3937.
(20) Linker, T. M.; Tiwari, S.; Kumazoe, H.; Fukushima, S.; Kalia, R. K.; Nakano, A.; Ramprasad, R.; Shimojo, F.; Vashishta, P. Field-Induced Carrier Localization Transition in Dielectric Polymers. *J. Phys. Chem. Lett.* **2020**, *11*, 352−358.
(21) Huan, T. D.; Mannodi-Kanakkithodi, A.; Kim, C.; Sharma, V.; Pilania, G.; Ramprasad, R. A Polymer Dataset for Accelerated Property Prediction and Design. *Sci. Data* **2016**, *3*, No. 160012.
(22) Mannodi-Kanakkithodi, A.; Huan, T. D.; Ramprasad, R. Mining Materials Design Rules from Data: The Example of Polymer Dielectrics. *Chem. Mater.* **2017**, *29*, 9001−9010.
(23) du, B. X.; Liang, H.; Li, J.; Zhang, C. Temperature Dependent Surface Potential Decay and Flashover Characteristics of Epoxy/SiC Composites. *IEEE Trans. Dielectr. Electr. Insul.* **2018**, *25*, 631−638.
(24) Shen, W.-W.; Mu, H.-B.; Zhang, G.-J.; Deng, J.; Tu, D.-M. Identification of Electron and Hole Trap Based on Isothermal Surface Potential Decay Model. *J. Appl. Phys.* **2013**, *113*, No. 083706.
(25) Zhou, C.; Chen, G. Space Charge and AC Electrical Breakdown Strength in Polyethylene. *IEEE Trans. Dielectr. Electr. Insul.* **2017**, *24*, 559.
(26) Fukushima, S.; Tiwari, S.; Kumazoe, H.; Kalia, R. K.; Nakano, A.; Shimojo, F.; Vashishta, P. Effects of Chemical Defects on Anisotropic Dielectric Response of Polyethylene. *AIP Adv.* **2019**, *9*, 45022.
(27) Cubero, D.; Quirke, N. Computer Simulations of Localized Small Polarons in Amorphous Polyethylene. *J. Chem. Phys.* **2004**, *120*, 7772.
(28) Chen, L.; Huan, T. D.; Quintero, Y. C.; Ramprasad, R. Charge Injection Barriers at Metal/Polyethylene Interfaces. *J. Mater. Sci.* **2016**, *51*, 506−512.
(29) Chen, L.; Huan, T. D.; Huzayyin, A.; Quintero, Y. C.; Ramprasad, R. First-Principles Study of Aluminum-Polyethylene Interfaces. In *2014 IEEE Conference on Electrical Insulation and Dielectric Phenomena (CEIDP)*, 2014; pp. 887−890.
(30) Chen, X.; Zhao, A.; Li, J.; Deng, J.; Zhang, G.; Zhao, X. First-Principle Investigation of the Charge Injection Barriers of Polyethylene and Polytetrafluoroethylene Oligomers. *J. Appl. Phys.* **2019**, *126*, No. 035101.
(31) Kohn; Sham, L. J. Self-Consistent Equations Including Exchange and Correlation Effects. *Phys. Rev.* **1965**, *140*, A1133−A1138.
(32) Car, R.; Parrinello, M. Unified Approach for Molecular Dynamics and Density-Functional Theory. *Phys. Rev. Lett.* **1985**, *55*, 2471−2474.
(33) Payne, M. C.; Teter, M. P.; Allan, D. C.; Arias, T. A.; Joannopoulos, J. D. Iterative Minimization Techniques For ab Initio total-Energy Calculations: Molecular Dynamics and Conjugate Gradients. *Rev. Mod. Phys.* **1992**, *64*, 1045.
(34) Perdew, J. P.; Burke, K.; Ernzerhof, M. Generalized Gradient Approximation Made Simple. *Phys. Rev. Lett.* **1996**, *77*, 3865.
(35) Blöchl, P. E. Projector Augmented-Wave Method. *Phys. Rev. B* **1994**, *50*, 17953−17979.
(36) Fujihira, M.; Inokuchi, H. Photoemission from Polyethylene. *Chem. Phys. Lett.* **1972**, *17*, 554−556.
(37) Hinuma, Y.; Grüneis, A.; Kresse, G.; Oba, F. Band Alignment of Semiconductors from Density-Functional Theory and Many-Body Perturbation Theory. *Phys. Rev. B* **2014**, *90*, No. 155405.
(38) Chen, G.; Zhao, J.; Li, S.; Zhong, L. Origin of Thickness Dependent DC Electrical Breakdown in Dielectrics. *Appl. Phys. Lett.* **2012**, *100*, 222904.
(39) Mulliken, R. S. Electronic Population Analysis on LCAO−MO Molecular Wave Functions. I. *J. Chem. Phys.* **1955**, *23*, 1833−1840.
(40) Wang, Y.; Nasreen, S.; Kamal, D.; Li, Z.; Wu, C.; Huo, J.; Chen, L.; Ramprasad, R.; Cao, Y. Tuning Surface States of Metal/Polymer Contacts Toward Highly Insulating Polymer-Based Dielectrics. *ACS Appl. Mater. Interfaces* **2021**, *13*, 46142−46150.
(41) Grimme, S. Semiempirical Gga-Type Density Functional Constructed with a Long-Range Dispersion Correction. *J. Comput. Chem.* **2006**, *27*, 1787.
(42) Krukau, A. V.; Vydrov, O. A.; Izmaylov, A. F.; Scuseria, G. E. Influence of the Exchange Screening Parameter on the Performance of Screened Hybrid Functionals. *J. Chem. Phys.* **2006**, *125*, 224106.
(43) Liechtenstein, A. I.; Anisimov, V. I.; Zaanen, J. Density-Functional Theory and Strong Interactions: Orbital Ordering in Mott-Hubbard Insulators. *Phys. Rev. B* **1995**, *52*, R5467−R5470.
(44) Shishkin, M.; Kresse, G. Self-Consistent GW Calculations for Semiconductors and Insulators. *Phys. Rev. B* **2007**, *75*, No. 235102.
(45) Shishkin, M.; Kresse, G. Implementation and Performance of the Frequency-Dependent *GW* Method within the PAW Framework. *Phys. Rev. B* **2006**, *74*, 35101.
(46) Shimojo, F.; Fukushima, S.; Kumazoe, H.; Misawa, M.; Ohmura, S.; Rajak, P.; Shimamura, K.; Bassman, L.; Tiwari, S.; Kalia, R. K.; Nakano, A.; Vashishta, P. QXMD: An Open-Source Program for Nonadiabatic Quantum Molecular Dynamics. *Software X* **2019**, *10*, No. 100307.
(47) Shimojo, F.; Ohmura, S.; Mou, W.; Kalia, R. K.; Nakano, A.; Vashishta, P. Large Nonadiabatic Quantum Molecular Dynamics Simulations on Parallel Computers. *Comput. Phys. Commun.* **2013**, *184*, 1−8.
(48) Meng, S.; Kaxiras, E. Real-Time, Local Basis-Set Implementation of Time-Dependent Density Functional Theory for Excited State Dynamics Simulations. *J. Chem. Phys.* **2008**, *129*, No. 054110.
(49) Shimojo, F.; Hattori, S.; Kalia, R. K.; Kunaseth, M.; Mou, W.; Nakano, A.; Nomura, K. I.; Ohmura, S.; Rajak, P.; Shimamura, K.; Vashishta, P. A Divide-Conquer-Recombine Algorithmic Paradigm for Large Spatiotemporal Quantum Molecular Dynamics Simulations. *J. Chem. Phys.* **2014**, *140*, No. 18A529.
(50) Runge, E.; Gross, E. K. U. Density-Functional Theory for Time-Dependent Systems. *Phys. Rev. Lett.* **1984**, *52*, 997−1000.
(51) Tully, J. C. Molecular Dynamics with Electronic Transitions. *J. Chem. Phys.* **1990**, *93*, 1061−1071.

https://doi.org/10.1021/acsami.1c14587
ACS Appl. Mater. Interfaces 2021, 13, 60393−60400

(52) Craig, C. F.; Duncan, W. R.; Prezhdo, O. V. Trajectory Surface Hopping in the Time-Dependent Kohn-Sham Approach for Electron-Nuclear Dynamics. *Phys. Rev. Lett.* **2005**, *95*, No. 163001.

https://doi.org/10.1021/acsami.1c14587
ACS Appl. Mater. Interfaces 2021, 13, 60393−60400